We are IntechOpen, the world's leading publisher of Open Access books Built by scientists, for scientists

4,800
Open access books available

122,000
International authors and editors

135M
Downloads

Our authors are among the

154
Countries delivered to

TOP 1%
most cited scientists

12.2%
Contributors from top 500 universities

CLARIVATE ANALYTICS BOOK CITATION INDEX INDEXED

WEB OF SCIENCE™

Selection of our books indexed in the Book Citation Index in Web of Science™ Core Collection (BKCI)

Interested in publishing with us?
Contact book.department@intechopen.com

Numbers displayed above are based on latest data collected.
For more information visit www.intechopen.com

12

Moving Target Detection and Velocity Estimation in Multi-Channel AT-InSAR Systems from Amplitude and Phase Data

Alessandra Budillon
Dipartimento per le Tecnologie - Università di Napoli "Parthenope"
Naples, Italy

1. Introduction

Recently, Along Track Interferometric Synthetic Aperture Radar systems (AT-InSAR) have been applied for traffic monitoring of ground vehicles (Meyer et al. 2006, Chapin & Chen, 2006, Hinz et al. 2007).
AT-InSAR systems are composed by more than one SAR antennas (typically two), mounted on the same platform and displaced along the platform moving direction. The separation distance between the antennas is denoted as baseline.
From the acquisitions of two or more image signals these systems are able to recover additional information about the observed scene: they allow the detection of moving targets on the ground and the estimation of their radial velocity (Raney, 1971). This is possible because the interferometric phase, i. e. the $(-\pi,\pi]$ wrapped phase of the signal obtained from the point to point correlation between the complex images acquired from the two interferometric antennas, is related to the radial velocity through a known mapping. Then, after the so-called Phase Unwrapping (PhU) operation, a map of the target range velocity can be retrieved.
Detection and radial velocity estimation of a ground moving target are challenging problems, due to the difficulty of separating the moving target signal from the stationary background (clutter) (Chiu, 2003). Several methods, based on very different approaches, have been proposed in literature, such as Displaced Phase Centre Antennas (DPCA systems) techniques (Gierull & Livingstone, 2004, Chiu & Livingstone 2005), and Space-Time Adaptive Processing (STAP) (Ender, 1999, Klemm, 2002, Gierull & Livingstone, 2004). Interest in investigating AT-InSAR processor is motivated since such alternative techniques attempt to reject or cancel the stationary clutter but have the drawback that can attenuate slowly moving targets (Chiu & Livingstone 2005).
AT-InSAR systems usually use only interferometric phase information in order to estimate radial velocity (Chen, 2004, Budillon et al. 2005, Budillon et al. 2008a) while complex data in place of phase-only data have already been used in AT-InSAR systems detection applications (Gierull, 2004, Zhang et al. 2005, Budillon et al., 2008b) showing that detection performance improve when complex data are used.

In this paper it is proposed to consider both amplitude and phase of the interferometric SAR image since in the case of target velocity estimation of not extended targets, the exploitation of the image amplitude together with the image phase can add more information, even if the amplitude is influenced in a less sensitive way with respect to the phase. AT-InSAR approach can be considered clutter-limited since when the signal to clutter ratio decreases, the velocity estimation becomes gradually more and more critical, till it fails completely. Moreover there are solution ambiguities than can keep the velocity estimation from working correctly due to the wrapped phase measurements.
In this paper both above mentioned problems are solved by using statistical estimation methods, and exploiting multi-channel interferograms. The statistical estimation methods allow taking into account the correct statistics of the involved noise (likelihood model). The use of a multi-channel interferogram, that in this case can be obtained exploiting frequency diversity and/or baseline diversity, has a twofold effect: multi-channel interferograms can help to reduce the variance of the estimation, and, if properly chosen, can allow avoiding solution ambiguities (Budillon et al. 2005, Budillon et al. 2008c).
It is shown that combining the real and imaginary part of more than two acquired images (multi-channel approach) produce significative improvements in the velocity estimation accuracy and a sensitive reduction in the false alarm rate compared with AT-InSAR conventional systems using phase-only data.
In section 2 the AT-InSAR statistical model has been presented and the joint interferogram amplitude and phase distribution has been derived. Based on this distribution, in section 3 a radial velocity estimation maximum likelihood approach using more interferogram channels has been reported. Cramer Lower Bounds and Root Mean Squared Error show the method performance on simulated data using Terra SAR-X parameters and are evaluated in the case of phase-only data and amplitude and phase data. In section 4 a likelihood ratio test is adopted to detect the moving target and performance detection in terms of Probability of detection and false alarm have been examined comparing results obtained on phase-only data and on amplitude and phase data. Moreover a multi-channel detection strategy is proposed and compared with the one based on a single interferogram. Finally follow conclusions in section 5.

2. AT-InSAR statistical model

In this section is presented the statistical model of the AT-InSAR signal. Consider an AT-InSAR system constituted by two antennas moving along the direction $\boldsymbol{x}$ (azimuth) (see Figure 1), and suppose that the two antennas are separated by a baseline b along the azimuth direction $\boldsymbol{x}$, such that $b \ll H$, where H is the platform quota. Assume a target on the ground moving with a constant velocity $\boldsymbol{v}_T = v_{Tx}\,\boldsymbol{x} + v_{Tr}\,\boldsymbol{r}$, where v_{Tx} and v_{Tr} are the velocity components along the azimuth and the line of sight direction (range) $\boldsymbol{r}$, respectively. The azimuth velocity component v_{Tx} produce a Doppler slope change causing a defocusing in the moving target image. The radial velocity component v_{Tr} produce a Doppler history different from that of the stationary background, and an azimuth displacement of the target.
Suppose that $|v_{Tx}|$, $|v_{Tr}| << |v_P|$, where $\boldsymbol{v}_P = v_P\,\boldsymbol{x}$ is the velocity of the flying platform and $H \gg X$ and $H \gg W$, where X and W are the antenna footprint dimensions.

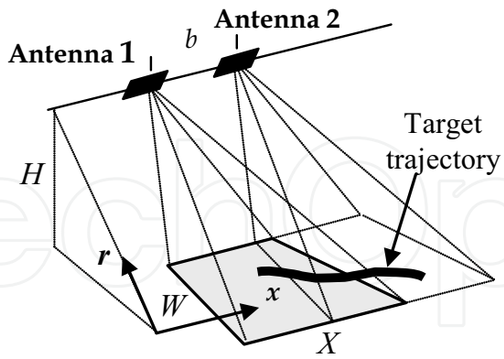

Fig. 1. Along-Track Interferometry system single baseline geometry

The SAR image signal formed by each antenna can be modeled as the superposition of the contributions of the moving target, of the stationary clutter, and of the additive noise. Then in a fixed image pixel we have:

$$Z_1 = \begin{cases} Z_{c1} + N_1 + Z_{T1} & \text{in presence of moving target } \mathrm{H}_1 \\ Z_{c1} + N_1 & \text{in absence of moving target } \mathrm{H}_0 \end{cases}$$
$$Z_2 = \begin{cases} Z_{c2} + N_2 + Z_{T2} & \text{in presence of moving target } \mathrm{H}_1 \\ Z_{c2} + N_2 & \text{in absence of moving target } \mathrm{H}_0 \end{cases} \quad . \tag{1}$$

Z_1 and Z_2 are the computed image signals in the considered pixel, Z_{c1} and Z_{c2} are the clutter signals acquired by the two antennas, N_1 and N_2 represent the receiver thermal noise, and Z_{T1} and Z_{T2} denote the SAR images of the moving target produced by the two interferometric antennas, which will exhibit a phase factor related to the radial velocity:

$$Z_{T1} = A_1 , \qquad Z_{T2} = A_2 \, e^{-j\phi_v} , \tag{2}$$

where A_1 and A_2 are the target images obtained for zero velocity, and ϕ_v is given by (Raney, 1971):

$$\phi_v = \left\langle \frac{4\pi b}{\lambda} \frac{v_r}{|v_P|} \right\rangle_{2\pi} = \left\langle \frac{4\pi b}{\lambda} u_r \right\rangle_{2\pi} , \tag{3}$$

where λ is the wavelength corresponding to the working frequency f=c/ λ of the SAR system, and $\langle \cdot \rangle_{2\pi}$ represents the "modulo-2π" operation. In (3) the normalized radial velocity $u_r = v_r / |v_P|$ has been also introduced. Where the moving target is present, $v_r \neq 0$ and consequently $\phi_v \neq 0$, otherwise the along-track inteferometric phase (3) is null. From (3) it is easy to derive that the ambiguity velocity value, such that the interferometric phase is equal

to ± π, is given by $u_{r,amb}$=± λ /(4b). For |u_r|> λ /(4b) the interferometric phase wraps, as evidenced also by the "*modulo*-2 π" operation. Also disturbing effects have to be taken into account, they are related to different parameters such as the signal to clutter ratio (SCR), the clutter to thermal noise ratio (CNR), and the clutter coherence γ_c. Since the time elapsing between the two interferometric acquisitions is very small (typically of the order of a millisecond) the clutter coherence can be considered equal to one. Then only the effect of SCR and CNR has to be considered.

To analyze the effect that the clutter and noise signals have on the velocity estimation accuracy, a statistical model for the involved signals has to be introduced. It is well known that the clutter signals Z_{c1} and Z_{c2} can be assumed random processes, whose real and imaginary parts are mutually uncorrelated Gaussian signals, with zero mean and same variance σ_c^2, since they are resulting from the superposition of the signals backscattered from many scattering centres lying in the resolution cell. N_1 and N_2 can be modelled as two additive (to the clutter) zero mean Gaussian complex processes independent of each other, independent on the clutter and with same variance $2\,\sigma_N^2$.

When the moving target is present, a deterministic model is applicable to the case of a target whose Radar Cross Section (RCS) can be expressed by a deterministic function of the incidence angle (Budillon et al., 2008a). This model applies to canonical scattering objects (such as corner reflectors, spheres, etc.), and to complex or extended targets whose RCS does not rapidly change between the interferometric acquisitions. An accurate knowledge of the average RCS values can be available only for accurately characterized targets (Palubinskas et al. 2004).

A Gaussian model for the target allows to take into account the lack of knowledge of the target RCS values (that can be described in terms of variance σ_T^2), and then of the SCR, and applies to complex or extended targets which can be considered to consist of a large number of isotropic scattering elements, randomly distributed in a region whose dimensions are large compared to the wavelength of the illuminating radiation, and all contributing to the overall signal with the same weight**.** In the following the target signals Z_{T1} and Z_{T2}, have been modelled as zero mean (complex) Gaussian processes.

Then, when the moving target is absent (Z_{T1} = Z_{T2} = *0*), the two processes Z_1 and Z_2 are Gaussian with zero-mean and correlation coefficient γ_{H0} given by:

$$\gamma_{H_0} = \frac{\mathrm{E}\left[\left(Z_{c1}+N_1\right)\left(Z_{c2}+N_2\right)^*\right]}{\sqrt{\mathrm{E}\left[\left|Z_{c1}+N_1\right|^2\right]\mathrm{E}\left[\left|Z_{c2}+N_2\right|^2\right]}} = \frac{\gamma_c}{\left(1+\dfrac{1}{\mathrm{CNR}}\right)}, \tag{4}$$

where $\mathrm{E}[\cdot]$ denotes the expectation operation, * denotes the conjugate, γ_c is the clutter coherence (real valued, in the ATI application can be considered equal to one), representing the correlation between images Z_{c1} and Z_{c2}, and CNR = σ_c^2 / σ_N^2, where $2\,\sigma_c^2$ and $2\,\sigma_N^2$ are the clutter and thermal noise powers respectively (the factor two is due to the sum of the powers of the real and imaginary parts).

Instead, when we are in presence of the moving target ($Z_{T1} \neq 0$, $Z_{T2} \neq 0$), the expression of correlation coefficient change with respect to (4) and γ_{H1} is given by:

$$\gamma_{H_1} = \frac{E\left[\left(Z_{c1}+N_1+Z_{T1}\right)\left(Z_{c2}+N_2+Z_{T2}\right)^*\right]}{\sqrt{E\left[\left|Z_{c1}+N_1+Z_{T1}\right|^2\right]\ E\left[\left|Z_{c2}+N_2+Z_{T2}\right|^2\right]}} = \\ = \frac{\gamma_c\sigma_c^2+\sigma_T^2\gamma_T}{\sigma_c^2+\sigma_n^2+\sigma_T^2} = \frac{\gamma_c+\gamma_T \mathrm{SCR}}{1+\frac{1}{\mathrm{CNR}}+\mathrm{SCR}}, \tag{5}$$

where $\mathrm{SCR} = \sigma_T^2/\sigma_c^2$, where $2\sigma_T^2$ is the target power, and γ_T is the target (complex) coherence that depends on the target velocity through the nominal phase (3):

$$\gamma_T = \frac{\mathrm{E}\left[Z_{T1}Z_{T2}^*\right]}{\sqrt{\mathrm{E}\left[\left|Z_{T1}\right|^2\right]\ \mathrm{E}\left[\left|Z_{T2}\right|^2\right]}} = \frac{E\left[A_1A_2^*\right]}{\sqrt{\mathrm{E}\left[\left|A_1\right|^2\right]\ \mathrm{E}\left[\left|A_2\right|^2\right]}} e^{j\varphi_v} = \gamma_A e^{j\varphi_v}, \tag{6}$$

where γ_A is the target coherence for zero radial velocity that is usually assumed equal to one.

The two processes $Z_1=Z_{1r}+jZ_{1i}$ and $Z_2=Z_{2r}+jZ_{2i}$ are Gaussian, then the joint probability density function of $\boldsymbol{Z}=[Z_{1r}\ Z_{2r}\ Z_{1i}\ Z_{2i}]^T$, is Gaussian with zero mean and covariance matrix

$$\boldsymbol{C} = \begin{cases} \boldsymbol{C}_c+\boldsymbol{C}_N & \mathrm{H}_0 \\ \boldsymbol{C}_c+\boldsymbol{C}_N+\boldsymbol{C}_T & \mathrm{H}_1 \end{cases}, \tag{7}$$

where the matrices $\boldsymbol{C}_c$, $\boldsymbol{C}_N$ and $\boldsymbol{C}_T$ are respectively the clutter, noise and target covariance matrix. It can be easily shown (Davenport & Root, 1958) that:

$$\boldsymbol{C} = \sigma^2 \begin{bmatrix} 1 & Re(\gamma) & 0 & -Im(\gamma) \\ Re(\gamma) & 1 & Im(\gamma) & 0 \\ 0 & Im(\gamma) & 1 & Re(\gamma) \\ -Im(\gamma) & 0 & Re(\gamma) & 1 \end{bmatrix}, \tag{8}$$

where, in the hypothesis H_0, has to be taken $\sigma^2 = \sigma_c^2 + \sigma_N^2$ and $\gamma=\gamma_{H0}$, in the hypothesis H_1, $\sigma^2 = \sigma_c^2 + \sigma_N^2 + \sigma_T^2$ and $\gamma=\gamma_{H1}$.

Then the joint probability density function of $\boldsymbol{Z}=[Z_{1r}\ Z_{2r}\ Z_{1i}\ Z_{2i}]^{\mathrm{T}}$, is Gaussian, i.e.

$$f_{\boldsymbol{Z}}(\boldsymbol{z}) = f_{Z_{1r},Z_{2r},Z_{1i},Z_{2i}}(z_{1r},z_{2r},z_{1i},z_{2i}) = \frac{1}{(2\pi)^2|\boldsymbol{C}|^{1/2}} \exp\left\{-\frac{1}{2}\boldsymbol{z}^{\boldsymbol{T}}\boldsymbol{C}^{-1}\boldsymbol{z}\right\}. \tag{9}$$

The SAR interferometric amplitude and phase distribution can be derived from (9) introducing the interferometric signal I:

$$I = Z_1Z_2^* = W\exp(j\Phi). \tag{10}$$

The joint W and Φ pdfs, in the hypothesis H_1 and H_0, derived from (9) via variables transformations (Davenport & Root, 1958), are respectively:

$$f_{W\Phi}(w,\phi;\mathrm{H}_1)=\frac{w}{2\pi\sigma_c^2\left(1+\frac{1}{\mathrm{CNR}}+\mathrm{SCR}\right)^2\left(1-|\gamma_{H1}|^2\right)}\cdot$$
$$K_0\left(\frac{w}{\sigma_c^2\left(1+\frac{1}{\mathrm{CNR}}+\mathrm{SCR}\right)\left(1-|\gamma_{H1}|^2\right)}\right)\exp\left\{\frac{|\gamma_{H1}|w\cos(\phi-\phi_o)}{\sigma_c^2\left(1+\frac{1}{\mathrm{CNR}}+\mathrm{SCR}\right)\left(1-|\gamma_{H1}|^2\right)}\right\}, \tag{11}$$

$$f_{W\Phi}(w,\phi;\mathrm{H}_0)=\frac{w}{2\pi\sigma_c^2\left(1+\frac{1}{\mathrm{CNR}}\right)^2\left(1-\gamma_{H0}{}^2\right)}\cdot$$
$$K_0\left(\frac{w}{\sigma_c^2\left(1+\frac{1}{\mathrm{CNR}}\right)\left(1-\gamma_{H0}^2\right)}\right)\exp\left\{-\frac{\gamma_{H0}w\cos(\phi)}{\sigma_c^2\left(1+\frac{1}{\mathrm{CNR}}\right)\left(1-\gamma_{H0}^2\right)}\right\}.$$

where K_0 denote the modified Bessel function of order zero, $w \geq 0, 0 \leq \phi \leq 2\pi$ and ϕ_0 is γ_{H1} phase. The analytical expressions of the pdfs ((9) and (11)) and of the coherences ((4) and (5)), reveal their dependence on CNR, SCR, radial velocity (trough the phase ϕ_v), clutter coherence γ_c and target coherence γ_A. As far as the coherence values are concerned, they are assumed equal to 1 in ATI applications.

In Figure 1 and Figure 2 the joint pdf of W and Φ, respectively in the hypothesis H_0 and H_1, with CNR= 10 dB, SCR= 10 dB), $u_r=u_{r,amb}/2$ corresponding to phase 1.5 rad, are shown.

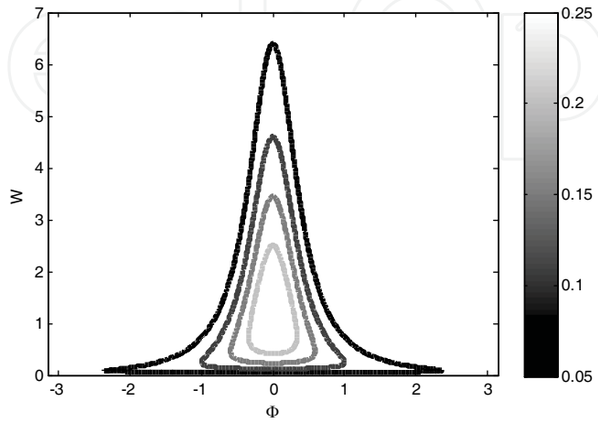

Fig. 2. Inteferogram joint amplitude phase pdf in the hypothesis H_0 for CNR=10 dB.

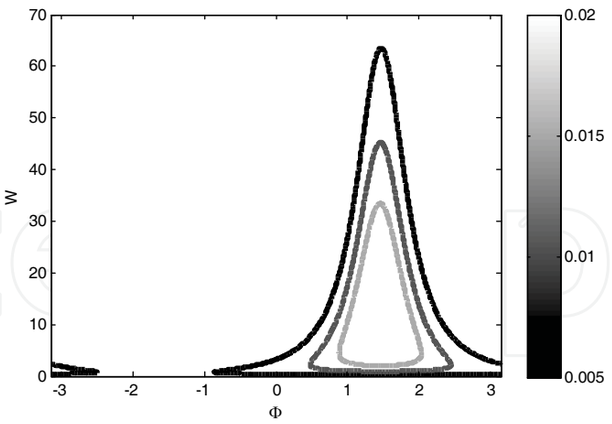

Fig. 3. Inteferogram joint amplitude phase pdf in the hypothesis H_1 for CNR= 10 dB, SCR= 10 dB, u_r=$u_{r,amb}/2$, corresponding to phase 1.5 rad.

3. Multi-Channel AT-InSAR moving target velocity estimation

3.1 Joint estimation of velocity and SCR via Maximum likelihood approach

Since interferometric phase is measured in the interval (-π,π], then a Phase Unwrapping (PhU) operation is required to retrieve the target radial velocity. The PhU operation presents solution ambiguities when only one phase interferogram (single-channel) is used. It has already been shown in (Budillon et al. 2005, Budillon et al. 2008c) that the joint use of multi-channel configurations (deriving from the use of more than two interferometric images acquired with different baselines or at different working frequencies) and of classical statistical estimation techniques allows to obtain very accurate solutions and to overcome the limitations due to the presence of ambiguous solutions, intrinsic in the single-channel configurations.

Different baseline data sets (at least two) can be generated when the AT-InSAR system is constituted by more than two antennas (at least three). Different frequency data sets can be generated in two ways. In the first, we can suppose that the SAR sensors can operate at different working frequencies, for instance in X and C bands simultaneously. In the second, the multi-frequency interferograms can be obtained by sub-band filtering the interferometric images splitting the overall bandwidth (Budillon et al. 2008c). Note that while the use of a different working frequency or baseline does not affect the SCR values, the generation of adding frequencies by partitioning the available band reduces the SCR value. This SCR reduction is in inverse relation to the number of looks, as the spatial resolution worsens increasing the number of looks.

Likelihood function is easily derived from either pdf (9) or (11) in the H_1 hypothesis. As discussed in the previous section, it depends on CNR, SCR and radial velocity since clutter and target coherence are assumed equal to 1 in ATI applications. CNR value can be easily computed from the data isolating an area where the target is absent. Then, the final estimation can be casted as a joint maximum likelihood estimation (Kay, 1993) of velocity and SCR:

$$\left[\hat{u}_r, \hat{SCR}\right] = \underset{u_r, SCR}{arg\,max}\, L(u_r, \mathrm{SCR})$$
$$L(u_r, SCR) = \prod_{k=1,\cdots,N} \underbrace{f_{\boldsymbol{Z}}\left(\mathbf{Z}(k) \middle| u_r, \mathrm{SCR}, \mathrm{H}_1\right)}_{\text{single channel likelihood function}} \quad , \tag{12}$$

where the samples $\{\boldsymbol{Z}(k)\}_{k=1,N}$ represent the SAR signals acquired in N channels. The factorization in (12) comes from the assumed statistical independence of the multi-channel interferograms.

3.2 Performance assessment

Estimation performance evaluation has been carried out using Terra SAR-X parameters in Table 1, but in order to consider a multi-channel system a second baseline b_2=1.8b_1 [m] (b_1=1.2 [m]), has been adjoined. By sub-band filtering the interferometric images also 4 azimuth looks have been considered, obtaining in total N=8 channels. The maximum normalized radial velocity value that can be unambiguously detected results $|u_{\mathrm{r,max}}|=\lambda/(4b)=6.5\times10\text{-}3$, corresponding to a not normalized velocity $|v_{r,amb}|$ of about 49.4 m/sec (178 Km/h).

TerraSAR-X	
Quota	514.8 Km
Platform velocity	7.6 Km/s
Along track antenna dimension	4.8 m
Across track antenna dimension	0.8 m
Along track baseline	1.2 m
Working frequency	X band– f_X=9.65 GHz
Wavelength	3.12 cm
Range bandwidth	150 MHz

Table 1. Main parameters of Terra SAR X system

To evaluate the performance of the ML estimator (12), the Cramer Rao Lower Bounds (CRLBs) (Kay, 1993) and the Root Mean Square Errors (RMSEs) for the unknown parameters (v_r, SCR) have been computed. CRLBs depend on the data model and represent the maximum accuracy attainable with given data. In order to point out the advantages of taking into account amplitude and phase information they have been compared with the ones obtained using a phase-only approach, i.e. a maximum likelihood estimation based on the phase-only distribution (Budillon et al. 2008a).

The $\mathrm{CRLB}^{1/2}$ relative to the not normalized radial velocity v_r and SCR are reported respectively in Figures 4 and 5. In Figure 4(a) it is shown the $\mathrm{CRLB}^{1/2}$ relative to the estimation of the not normalized radial velocity v_r, Vs. the radial velocity and relevant to the model based on phase-only data. It is evident the significative improvements in the maximum accuracy attainable using the amplitude and phase model reported in Figure 4(b). The $\mathrm{CRLB}^{1/2}$ have been evaluated numerically and for different values of v_r in the range (0,

$v_{r,amb}$), for CNR=10 dB, and varying SCR (0,5,10,15,20 dB). It can be appreciated that as expected the CRLB$^{1/2}$ are lower for higher SCRs.

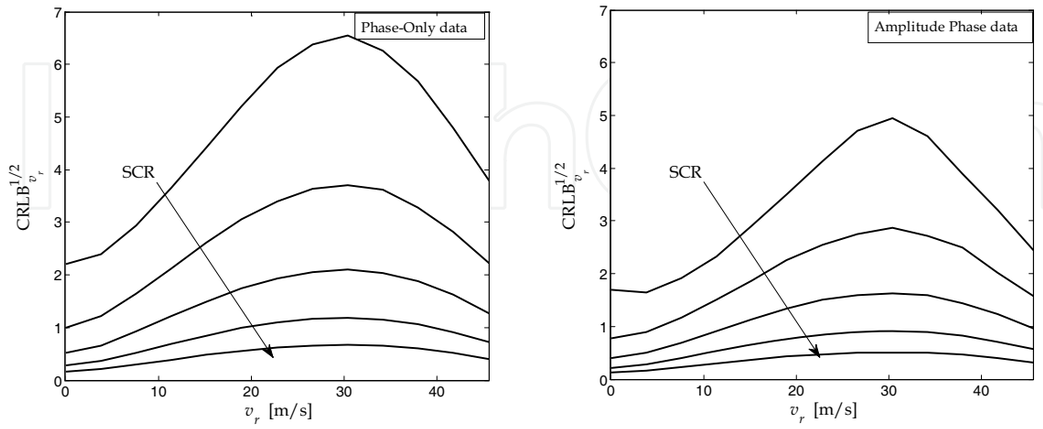

(a) (b)

Fig. 4. CRLB$^{1/2}$ relative to the estimation of the radial velocity v_r, Vs. the radial velocity and relevant to the model based on phase-only data (a) and to the model based on amplitude and phase data (b), for CNR=10 dB, and varying SCR (0,5,10,15,20 dB) .

In Figure 5(a) the CRLB$^{1/2}$ relative to the estimation of the SCR, Vs. the SCR and relevant to the model based on phase-only data is shown. Also for this parameter it is evident the significative improvements in the maximum accuracy attainable using the amplitude and phase model reported in Figure 5(b). Moreover it can be seen that using the amplitude and phase model the accuracy is slightly dependent on the SCR values, in both case the CRLB$^{1/2}$ is smaller for higher values of radial velocities, i.e. as expected it is easier to estimate the SCR of a faster target. In Figure 6(a) are shown the CRLB$^{1/2}$ and the RMSE relative to the estimation of the not normalized radial velocity v_r, Vs. the radial velocity and relevant to the model based on phase-only data, for CNR=10 dB, and SCR=10 dB. They can be compared with the correspondent CRLB$^{1/2}$ and the RMSE relevant to the model based on amplitude and phase data in Figure 6(b). It is noticeable that the performances are improved and also the RMSE is closer to the CRLB$^{1/2}$ when the estimation is based on the amplitude and phase model. In Figures. 7(a) and 7(b) the statistical mean values and the RMSEs for different estimated velocities in the range (0, $v_{r,amb}$), for CNR=10 dB and SCR=10 dB, respectively for the model based on phase-only data and to the model based on amplitude and phase data, are reported. Finally in Figures. 8(a) and 8(b) CRLB$^{1/2}$ and the RMSE relative to the estimation of SCR, Vs. the radial velocity are shown respectively for the two models. It is evident again the improvement attainable in case it is assumed the amplitude and phase model.

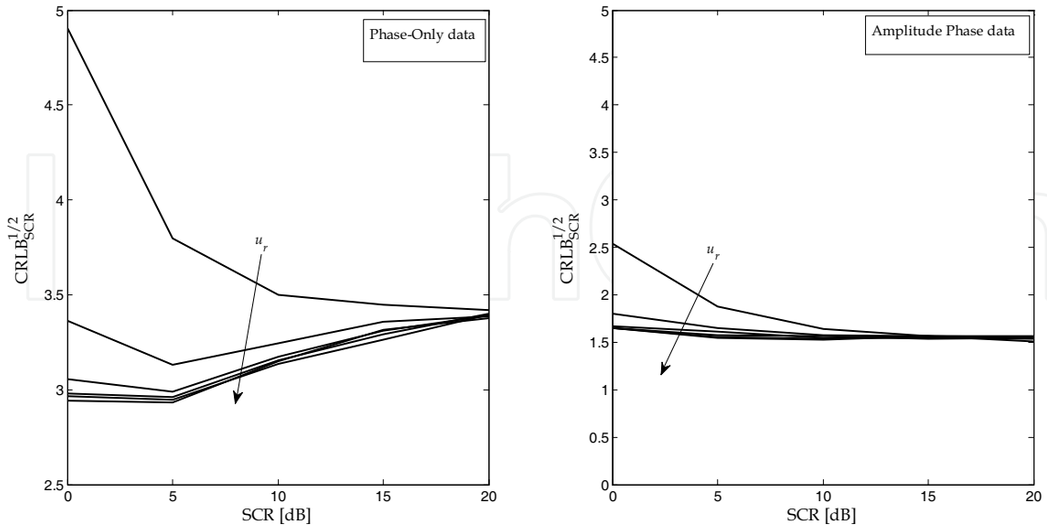

(a) (b)

Fig. 5. $CRLB^{1/2}$ relative to the estimation of SCR,Vs. SCR and relevant to the model based on phase-only data (a) and to the model based on amplitude and phase data (b), for CNR=10 dB, and varying v_r in the range (0, $v_{r,amb}$).

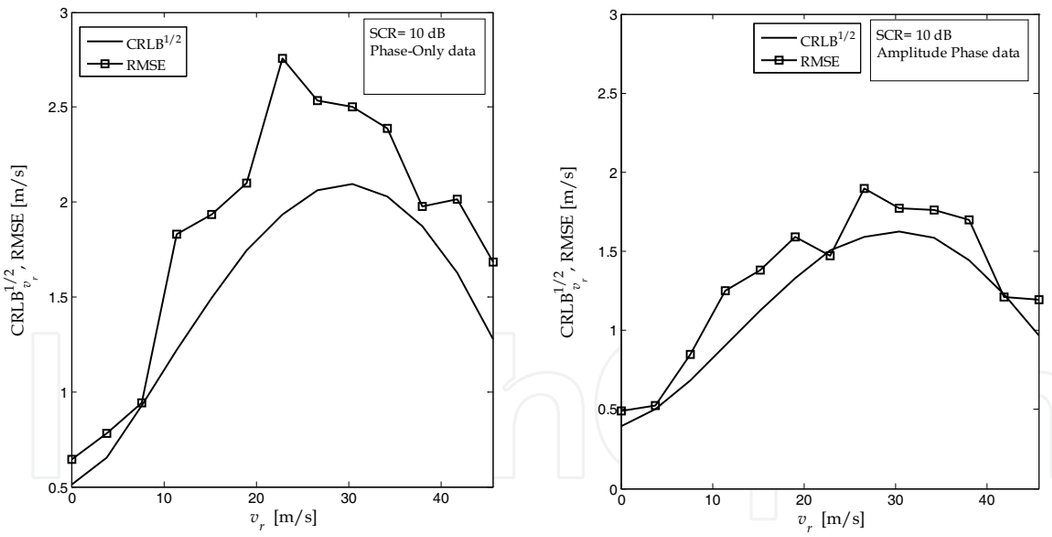

(a) (b)

Fig. 6. $CRLB^{1/2}$ and RMSE relative to the estimation of the radial velocity v_r,Vs. the radial velocity and relevant to the model based on phase-only data (a) and to the model based on amplitude and phase data (b), for CNR=10 dB, and SCR=10 dB.

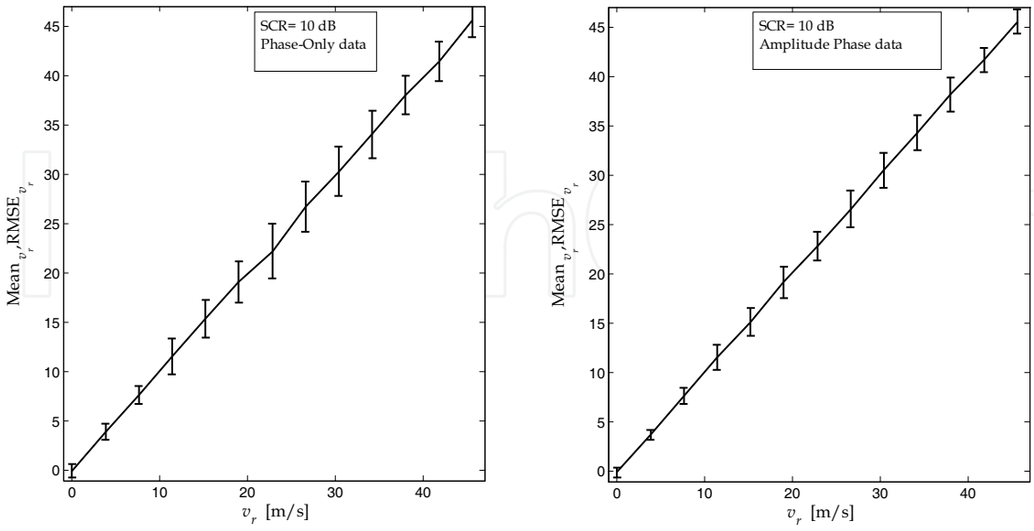

(a) (b)

Fig. 7. Mean value and RMSE relative to the estimation of the radial velocity v_r,Vs. the radial velocity and relevant to the model based on phase-only data (a) and to the model based on amplitude and phase data (b), for CNR=10 dB, and SCR=10 dB.

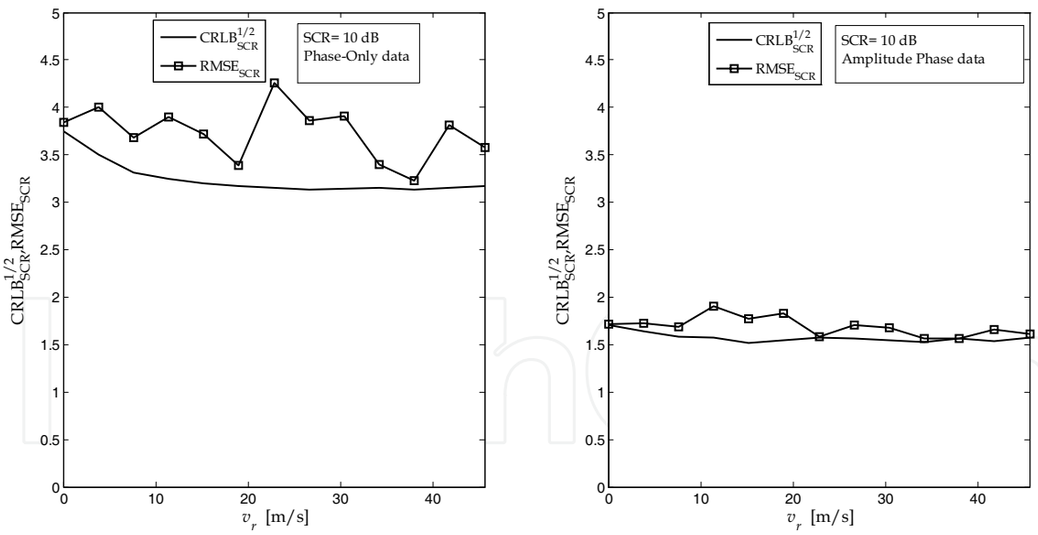

(a) (b)

Fig. 8. CRLB$^{1/2}$ and RMSE relative to the estimation of SCR,Vs. the radial velocity and relevant to the model based on phase-only data (a) and to the model based on amplitude and phase data (b), for CNR=10 dB, and SCR=10 dB.

4. Multi-Channel AT-InSAR moving target detection

4.1 Likelihood ratio test

A moving target can be detected in the conventional way by comparing the interferometric phase ϕ with a threshold η_T in the interval $(-\pi,\pi]$.

The performance of the detection process can be evaluated using the interferometric phase statistics (Budillon et al. 2088a). They are, as expected, better for high values of SCR, i.e. when the moving targets power is significantly larger than the clutter power. For moving targets mingling with the background clutter, the detection capability worsen, so that if one wants low values of P_{FA}, the P_D can decrease to very low values, not consistent with the applications.

As in the case of the velocity estimation (see Section 3) both amplitude and phase of the interferogram are considered instead of taking into account only the interferometric phase. Based on the pdfs (11) a constant false alarm rate (CFAR) detector can be designed.

In order to detect a moving target a likelihood ratio test is proposed, likelihood is derived from (11):

$$\Lambda(z)=\frac{f_{W\Phi}\left(w,\phi;\hat{u}_r,\hat{\mathrm{SCR}},\mathrm{H}_1\right)}{f_{W\Phi}\left(w,\phi;\mathrm{H}_0\right)}\underset{\mathrm{H}_1}{\overset{\mathrm{H}_0}{\lessgtr}}\eta\,. \tag{13}$$

Probability of false alarm P_{FA} and Probability of detection P_D are derived from (13)

$$\begin{aligned}\mathrm{P}_{FA}&=Pr\{\Lambda\geq\eta;\mathrm{H}_0\}\\ \mathrm{P}_D&=Pr\{\Lambda\geq\eta;\mathrm{H}_1\}\end{aligned}\quad. \tag{14}$$

The threshold η depends on a fixed P_{FA} .

4.2 Performance assessment

The detection performance evaluation has been carried out using the same multi-channel system presented in section 3.2.

The proposed approach provides curves of separation between the two classes (see Figure 9-10). In Figure 9 the separation curve for the two hypothesis, presence and absence of a moving target, has been evaluated for CNR=10 dB, SCR=10 dB, $u_r=u_{r,amb}/2=3.25\times10^{-3}$ (corresponding to the nominal noise-free value $\phi_o=\pi/2$), a threshold has been chosen such that P_D=0.91 and P_{FA}=0.001. Figure 10 shows the separation curve for the two hypothesis for CNR=10 dB, SCR= 0 dB, $u_r=u_{r,amb}/2=3.25\times10^{-3}$, a threshold has been chosen such that P_D=0.7 and P_{FA}=0.05.

For comparison with the conventional interferometric approach, the two Receiver Operating Characteristics (ROC) have been derived in both case SCR= 10 dB and SCR= 0 dB, for the amplitude and phase approach (solid line) and for the phase-only case (dashed line) (see Figure 11). It is clear the advantage in considering both amplitude and phase, for a fixed P_{FA} a higher P_D can be obtained.

In Figure 12 it can be appreciated the ROC dependence, in the amplitude and phase approach, on the radial velocity (Figure 12(a)), for CNR=10 dB, SCR=10 dB and on SCR

(Figure 12 (b)), for CNR=10 dB and $u_r=u_{r,amb}/2$. As expected it is easier to detect a faster and stronger (in terms of reflectivity) target.
In order to exploit the multi-channel interferograms in the detection process, suppose that the detection probability of one of the channel corresponding to the first baseline is equal to P_{D1}, and that the detection probability of one of the channel corresponding to the second baseline is equal to P_{D2}.
The probability that the target is detected from (N/2+j) channels (j=1,…,N/2) on a total of N channels results:

$$P_j = \sum_{k=j}^{N/2}\left[\binom{N/2}{k}P_{D1}^{k}\left(1-P_{D1}\right)^{N/2-k}\right]\left[\binom{N/2}{N/2-k+j}P_{D2}^{N/2-k+j}\left(1-P_{D2}\right)^{k-j}\right]. \quad (15)$$

The proposed multi-channel detection strategy consists in considering the moving target present when the majority of the interferogram values are above prefixed thresholds, so that the detection probability results:

$$P_{D>N/2} = \sum_{j=1}^{N/2} P_j \,. \quad (16)$$

For the estimation of the false alarm probability can be used the same reasoning.
In Figure 13 the ROC in the multi-channel amplitude phase approach (solid line) for CNR=10 dB, SCR=10 dB, N=8 interferograms compared with the single channel amplitude phase approach is reported (dashed lines). It is evident the advantages in considering a multi-channel approach that allows to keep low P_{FA} and at the same time high P_D.

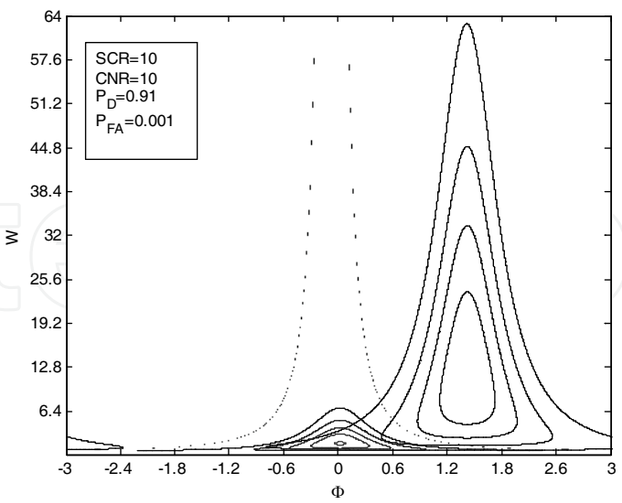

Fig. 9. Inteferogram joint amplitude phase pdf in the hypothesis H_0 and H_1 for $u_r=u_{r,amb}/2$, CNR=10 dB, SCR=10 dB, and the separation curve.

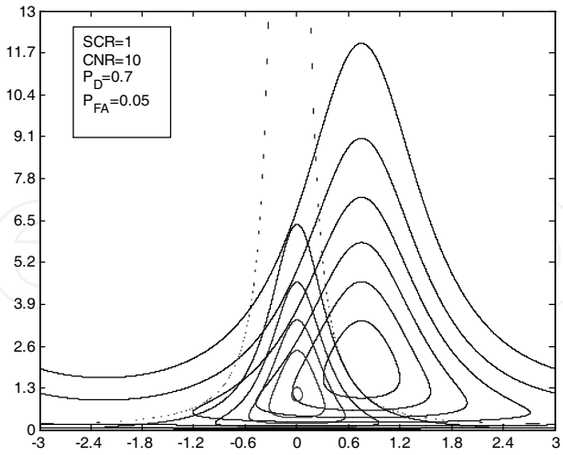

Fig. 10. Inteferogram joint amplitude phase pdf in the hypothesis H_0 and H_1 for $u_r=u_{r,amb}/2$, CNR=10 dB, SCR=0 dB, and the separation curve.

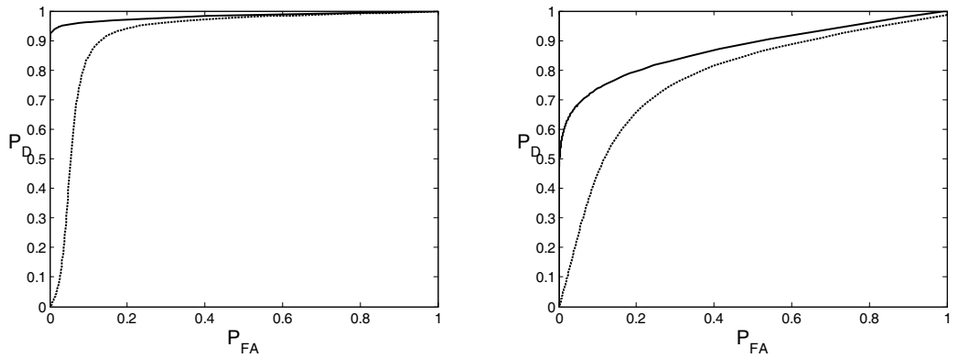

Fig. 11. ROC in the amplitude phase approach (solid line) and in the phase-only approach (dashed line) for $u_r=u_{r,amb}/2$, CNR=10 dB, SCR=10dB (a) and SCR=0 dB (b).

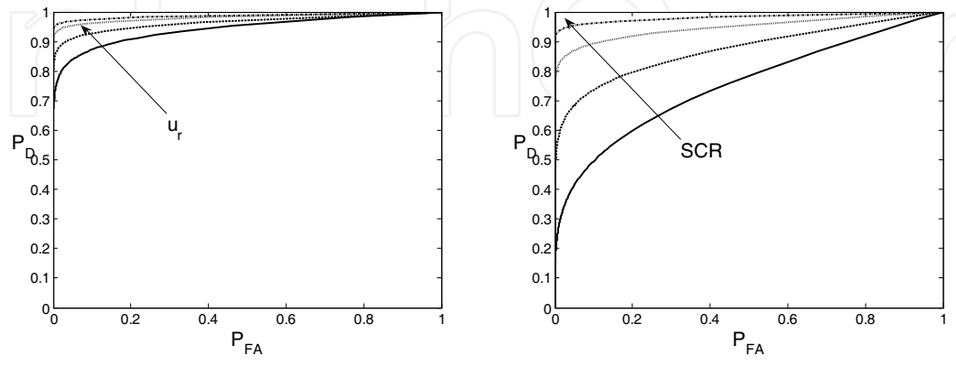

Fig. 12. ROC in the amplitude phase approach for CNR=10 dB, SCR=10 dB, varying u_r in the range (0, $u_{r,amb}$) (a) and for $u_r=u_{r,amb}/2$, varying SCR (-5 dB, 0 dB, 5 dB, 10 dB) (b).

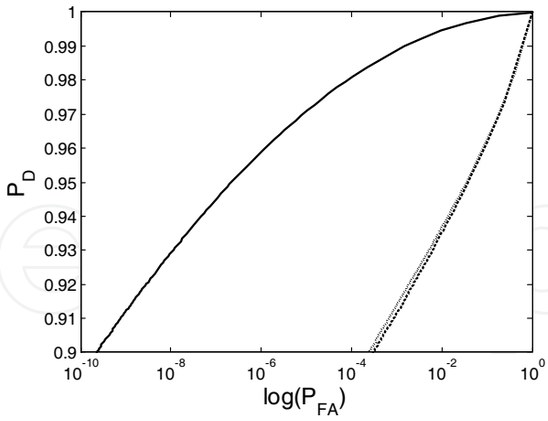

Fig. 13. ROC in the multi-channel amplitude phase approach (solid line) for CNR=10 dB, SCR=10 dB, N=8 interferograms compared with the single channel amplitude phase approach (dashed line baseline b_1 dotted line baseline b_2).

5. Conclusion

In this paper it has been presented the performance evaluation of multi-channel AT-InSAR systems, exploiting both amplitude and phase interferogram information, in terms of target radial velocity estimation accuracy and moving target detection ability.

A Gaussian target response model has been considered and the amplitude and phase joint pdf of the inteferogram has been derived. Based on this model a maximum likelihood approach has been used to estimate the target radial velocity. A comparison of the proposed approach with a phase-only system has been reported considering different system parameters, such as radial velocity, SCR, CNR. It reveals the benefits in exploiting both amplitude and phase interferogram information in terms of CRLB and RMSE. The analysis has been performed considering a multi-channel system based on the Terra SAR-X parameters but with a second baseline.

A constant false alarm rate (CFAR) detector has been considered. This approach provides curves of separation between the two classes, hypothesis H_0, and H_1, in order to detect the pixels in the SAR images where a moving target is present. The proposed approach outperforms the conventional phase-only approach and in particular is able to detect target with low SCR. ROCs have been presented varying SCR and the normalized radial velocity.

Regarding the detection process, the use of multi-channel interferograms, after the application of a threshold stage to each channel, allows to adopt a binary integration to combine single-channel decisions. Such a strategy, compared with the one based on a single interferogram, provides better results in terms of simultaneous low values of P_{FA} and high values of P_D.

6. References

Budillon, A.; Ferraiuolo, G.; Pascazio, V. & Schirinzi, G. (2005). "Multi-Channel SAR Interferometry via Classical and Bayesian Estimation Techniques", *J. of Applied Signal Processing*, vol. 20, pp. 3180-3193.

Budillon, A.; Pascazio, V. & Schirinzi, G. (2008a). "Estimation of Radial Velocity of Moving Targets by Along-Track Interferometric SAR Systems", *IEEE Geosci. Remote Sensing Letters*, vol. 5, pp. 349-353.

Budillon, A.; Pascazio, V. & Schirinzi, G. (2008b). "Moving Target Detection in Along Track SAR Interferometry from In-Phase and Quadrature Components Data", in *Proc. of IEEE International Geoscience and Remote Sensing Symposium (IGARSS'08)*, pp. III - 1178 - III - 1181.

Budillon, A.; Pascazio, V. & Schirinzi, G. (2008c). "Multichannel Along-Track Interferometric SAR Systems: Moving targets Detection and Velocity Estimation", *International Journal of Navigation and Observation*, Vol. 2008, 16 pp.

Chapin, E. & Chen, C.W. (2006). "GMTI Along-Track Interferometry Experiment", *IEEE Aerosp. Electronic Syst. Mag.*, vol. 21, pp. 15-20.

Chen, C.W. (2004). "Performance Assessment of Along-Track Interferometry for Detecting Ground Moving Targets", in *Proc. of 2004 IEEE Radar Conference*, pp. 99-104.

Chiu, S. (2003). "Clutter effects on ground moving target velocity estimation with SAR along-track interferometry", in *Proc. of 2003 IEEE International Geoscience and Remote Sensing Symposium (IGARSS '03),* Toulouse (France), vol. 2, pp. 1314-1319.

Chiu, S. & Livingstone, C. (2005). "A comparison of displaced phase centre antenna and along-track interferometry techniques for RADARSAT-2 ground moving target indication", *Can. J. Remote Sensing*, vol. 31, No. 1, pp. 37–51.

Davenport, W.B. & Root, W.L. (1958). *An Introduction to the Theory of Random Signals and Noise*, McGraw-Hill, Kogakusha,

Ender, J.H.G. (1999). "Space-Time Processing for Multichannel Synthetic Aperture Radar", IEE *Electronics & Communication Engineering Journal*, vol. 11, pp. 29-38.

Gierull, C.H. (2004). "Statistical Analysis of Multilook SAR Interferograms for CFAR Detection of Ground Moving Targets," *IEEE Trans. Geosci. Remote Sensing*, vol. 42, pp. 691-701.

Gierull, C.H. & Livingstone, C. (2004). "SAR-GMTI concept for RADARSAT-2" in *Applications of Space-Time Adaptive Processing,* R. Klemm (Ed.), IEE Publishers, London, UK.

Hinz, S.; Meyer, F.; Eineider, M. & Bamler, R. (2007). "Traffic Monitoring with Spaceborne SAR—Theory, Simulations, and Experiments", *Computer Vision and Image Understanding*, vol. 106, pp. 231-244.

Kay, S.M. (1993). *Fundamentals of Statistical Signal Processing: Vol. I, Estimation Theory*, Prentice-Hall.

Klemm, R.K. (2002). *Principles of space-time adaptive processing*, 2nd edn, London: IEE.

Meyer, F.; Hinz, S.;Laika, A.; Weihing, D. & Bamler, R. (2006). "Performance Analysis of the TerraSAR-X Traffic Monitoring Concept", *ISPRS J. of Photogr. and Remote Sensing*, vol. 61(3/4), pp 225-242.

Palubinskas, G.; Runge, H. & Reinartz, P. (2004). "Radar signatures of road vehicles", In *Proc. of 2004 IEEE International Geoscience and Remote Sensing Symposium (IGARSS '04),* Anchorage (USA), vol. 2, pp. 1498-1501.

Raney, R. (1971). "Synthetic Aperture Imaging Radar and Moving Targets", *IEEE Trans Aerosp. Electron. Syst*, vol. 7, pp. 499-505.

Zhang, Y.; Hajjari, A.; Kim, K. & Himed, B. (2005). "A Dual-Threshold ATI-SAR Approach for Detecting Slow Moving Targets", in *Proc. of 2005 IEEE Radar Conference*, pp. 295-299.

Geoscience and Remote Sensing

Edited by Pei-Gee Peter Ho

ISBN 978-953-307-003-2
Hard cover, 598 pages
Publisher InTech
Published online 01, October, 2009
Published in print edition October, 2009

Remote Sensing is collecting and interpreting information on targets without being in physical contact with the objects. Aircraft, satellites ...etc are the major platforms for remote sensing observations. Unlike electrical, magnetic and gravity surveys that measure force fields, remote sensing technology is commonly referred to methods that employ electromagnetic energy as radio waves, light and heat as the means of detecting and measuring target characteristics. Geoscience is a study of nature world from the core of the earth, to the depths of oceans and to the outer space. This branch of study can help mitigate volcanic eruptions, floods, landslides ... etc terrible human life disaster and help develop ground water, mineral ores, fossil fuels and construction materials. Also, it studies physical, chemical reactions to understand the distribution of the nature resources. Therefore, the geoscience encompass earth, atmospheric, oceanography, pedology, petrology, mineralogy, hydrology and geology. This book covers latest and futuristic developments in remote sensing novel theory and applications by numerous scholars, researchers and experts. It is organized into 26 excellent chapters which include optical and infrared modeling, microwave scattering propagation, forests and vegetation, soils, ocean temperature, geographic information , object classification, data mining, image processing, passive optical sensor, multispectral and hyperspectral sensing, lidar, radiometer instruments, calibration, active microwave and SAR processing. Last but not the least, this book presented chapters that highlight frontier works in remote sensing information processing. I am very pleased to have leaders in the field to prepare and contribute their most current research and development work. Although no attempt is made to cover every topic in remote sensing and geoscience, these entire 26 remote sensing technology chapters shall give readers a good insight. All topics listed are equal important and significant.

InTech Europe
University Campus STeP Ri

InTech China
Unit 405, Office Block, Hotel Equatorial Shanghai

Slavka Krautzeka 83/A
51000 Rijeka, Croatia
Phone: +385 (51) 770 447
Fax: +385 (51) 686 166
www.intechopen.com

No.65, Yan An Road (West), Shanghai, 200040, China
中国上海市延安西路65号上海国际贵都大饭店办公楼405单元
Phone: +86-21-62489820
Fax: +86-21-62489821

IntechOpen

IntechOpen